Miner Petrol (2009) 95:1–15
DOI 10.1007/s00710-008-0028-z

ORIGINAL PAPER

Raman spectroscopy of pure H_2O and NaCl-H_2O containing synthetic fluid inclusions in quartz—a study of polarization effects

M. Baumgartner · R. J. Bakker

Received: 9 September 2008 / Accepted: 23 September 2008 / Published online: 24 October 2008

Abstract The O-H stretching region of the Raman spectrum of aqueous solutions (H_2O-NaCl mixtures) is a set of poorly defined broad bands between 2,800cm^{-1} and 3,800cm^{-1}. The morphology of this spectral region is systematically characterised by deconvolution, using three Gaussian–Lorentzian contributions. This method allows a purely geometrical description of the spectra of pure H_2O as well as saline solutions at room temperatures. A pure H_2O reference solution has peak positions at 3,223cm^{-1} (*Peak1*), 3,433cm^{-1} (*Peak2*) and 3,617cm^{-1} (*Peak3*). The morphology of the Raman bands is influenced by the presence of NaCl in the aqueous solution. The variation in *Peak1* values is correlated with the salinity of the aqueous solutions according to the equation:

$$\Delta \nu_1 = 3222.8 + 1.69\, sal$$

where *sal* is the salinity (in mass%) and $\Delta\nu_1$ is the relative wavenumber (cm^{-1}) of *Peak1*. The contours of the Raman spectra of aqueous solutions in fluid inclusions in quartz are influenced by the birefringence of the host crystal, the orientation of the quartz-fluid interface, and the depth of the inclusion. The variation in *Peak1* due to birefringence is 3,220cm^{-1} to 3,239cm^{-1} using a polarised laser beam. Reflection polarisation caused by the orientation of the quartz-fluid interface results in a variability of 14cm^{-1}, independently from the orientation of the indicatrix. The effect of birefringence is reduced with increasing depth.

The Raman spectra of aqueous solutions in natural fluid inclusions can be used to calculate the salinity (in mass% NaCl) if the host quartz can be orientated with its optical axis parallel to the polarisation plane of the laser. Raman equipment that does not offer this possibility still can be used to analyse the salinity: multiple spectra must be acquired over at least 90° rotation of the sample; the lowest value of the deconvolved Gaussian–Lorentzian contribution of *Peak1* is a measure of the salinity.

Editorial handling: J.G. Raith

M. Baumgartner · R. J. Bakker (✉)
Department of Applied Geosciences and Geophysics,
Mineralogy and Petrology, University of Leoben,
Peter-Tunner-Str. 5,
A-8700 Leoben, Austria
e-mail: ronald.bakker@mu-leoben.at

Introduction

Knowledge of the salinity of fluid inclusions, including the type of salts and their amounts, is of importance for the interpretation of geological fluids and their role in rock-forming processes like diagenesis, metamorphism, and hydrothermal processes (e.g. Roedder 1984). One of the most important binary fluid systems for understanding geological processes is the NaCl-H_2O system. Raman spectroscopy offers a powerful tool for the investigation of the aqueous phase in fluid inclusions (e.g. Burke 2001) and can provide insights into vibrational modes of H_2O molecules. The liquid water spectrum can be strongly influenced by temperature and dissolved ions (e.g. Ratcliffe and Irish 1982; Rull and de Saja 1986; Frantz et al. 1993). Raman spectroscopy at selected low temperatures (down to −190°C) can be used to identify salt hydrates in frozen inclusions (e.g. Dubessy et al. 1982; Dubessy et al. 1992; Bakker 2004). The salinity of fluid inclusions is normally indirectly determined with microthermometry by measuring melting temperatures of, for example, ice, salt-hydrates or salts in the presence of a vapour phase. However, the presence of metastable phase assemblages can lead to erroneous estimations of salinity. The combination of

Raman spectroscopy with microthermometry offers new possibilities to identify the salinity and phase changes in those fluid inclusions (e.g. Bakker 2004).

The present study provides a method for analysing the Raman spectra of synthetic pure water and saline fluid inclusions at room temperature using Gaussian–Lorentzian functions that deconvolve the spectroscopic signal, i.e. the fitting of multiple spread functions to obtain hidden peaks (PeakFit 2002 4.11, user manual). The deconvolved spectra are evaluated to the use as a spectroscopic methodology to determine the salinity of natural aqueous fluids.

The Raman spectrum of H_2O can be substantially different between a free drop of water and a fluid inclusion as a result of polarisation effects (e.g. Dubessy et al. 2002). The Raman spectra of aqueous solutions in fluid inclusions may be influenced by the crystallographic orientation of the host mineral, due to the interaction between light (laser) and a birefringent mineral such as quartz (e.g. Turrell and Corset 1996). The spectral slopes in Fig. 1 in the range of 2,800cm^{-1} to 3,800cm^{-1} relative wavenumbers ($\Delta\nu$) for the enclosed fluid compared to that of a free water drop of the same composition depends on the orientation of the host quartz. Another polarisation effect to investigate is caused by the quartz-fluid inclusion interface, i.e. polarisation due to reflection. There are effects due to the angle between the plane of polarisation of the laser and the plane defined by the inclusion wall onto which the laser is incident (Fig. 2). The slope of the Raman spectrum is much steeper for the fluid in an inclusion than for a free water drop. For the same crystallographic orientation of the quartz host, an approximately perpendicular interface, i.e. parallel to the sample surface (arrow "*b*" in Fig. 2), results in a steeper spectral slope than for an inclined interface (arrow "*a*" in Fig. 2). These two polarisation effects on a laser beam crossing the quartz host in order to characterise the fluid entrapped in inclusions are also experimentally examined and quantified in this study.

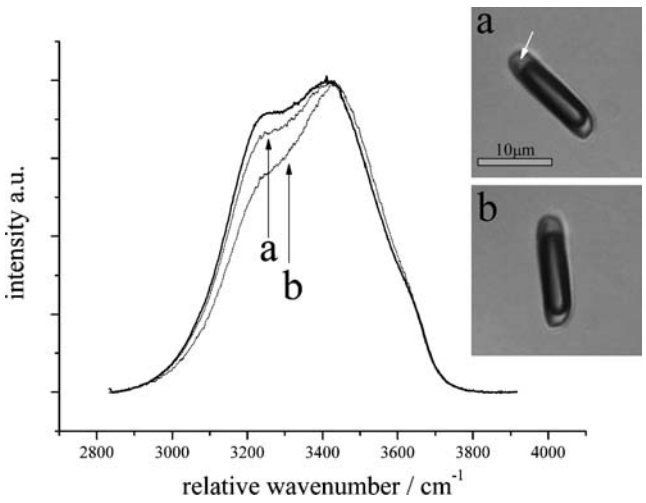

Fig. 1 Raman spectra of pure liquid water at 22°C measured in a synthetic fluid inclusion with different crystallographic orientations of the host mineral compared to a liquid water spectrum (thick line) measured in a free water drop. The arrow illustrates the spot of measurement within the inclusion. The spectrum labelled *a* was measured at the location shown by the arrow in the inclusion in the image, whereas the spectrum labeled *b* was measured at the same point, but after 40° rotation of the sample

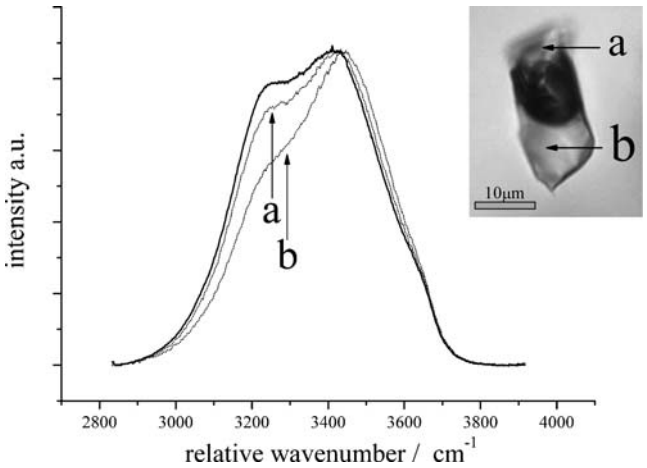

Fig. 2 Raman spectra of pure liquid water at 22°C measured in a synthetic fluid inclusion in quartz at two different locations at the interface (marked with arrows *a* and *b*, respectively) compared to the liquid water spectrum (thick line) measured in a free water drop. Measurements were taken at the same crystallographic orientation of the quartz host crystal

O-H "Stretching" Raman bands

Dissolved salts in fluid inclusions are normally characterised by freezing point depression of the aqueous solution. However, microthermometry does not uniquely identify the anions and cations in the solution. Theoretically, eutectic temperatures can be used to identify the salt component in binary systems with H_2O, although, these temperatures are difficult to measure accurately. Furthermore, in natural multi-component salt-H_2O systems the eutectic temperatures are unknown. Dissolved electrolytes that are present as mono-atomic ions are not Raman active, but they can influence the characteristic Raman bands of the solvent, i.e. the aqueous solution. The most informative region of the Raman spectrum of water is the "stretching"[1] region between 2,800cm^{-1} and 3,800cm^{-1} (e.g. Walrafen 1962). This region shows a broad undulating elevated signal, which is a complex profile of overlapping bands. These bands can be defined according to a variety of theoretical

[1] The vibration modes of a water molecule, i.e. a nonlinear triatomic molecule, are always composites of simultaneous stretching and bending of bonds.

vibrational modes such as unperturbed-, symmetric-, antisymmetric-, bending-vibrations and overtones. Multiple Gaussian–Lorentzian functions can be used to deconvolve this composite spectrum. However, many possibilities for fitting this "stretching" region are published in the literature: five deconvolved Gaussian components are defined by e.g. Carey and Korenowski (1998), Furić et al. (2000), Li et al. (2004), and Chumaevskii et al. (2001); four components are defined by e.g. Rull (2002); and three components are defined by e.g. Gopalakrishnan et al. (2005). Therefore, the spectral analyses of the "stretching" region are far from straightforward.

The contour of the Raman spectrum can be described by purely geometrical properties, such as amplitude (intensity), area, and slope (first derivate) in a wavenumber vs. intensity diagram (e.g. Mernagh and Wilde 1989; Furić et al. 2000). Bakker (2004) recommends a purely geometrical fit of the Raman water spectrum with three Gaussian–Lorentzian contributions with signal positions at 3,222cm^{-1}, 3,433cm^{-1}, and 3,617cm^{-1}. This approach is an unambiguous procedure for fitting spectra and allows a relative easy comparison of peak positions and changes in spectrum morphology among aqueous solutions of different salinities.

The structure of liquid water is significantly altered if charged ions, which interact with the permanent dipole moments of the water molecule, are present. With increasing number of cations and anions in the solution, this liquid structure becomes more and more coordinated (e.g. Rull and de Saja 1986). The positions and intensities of the deconvolved peaks in the OH stretching band can be related to the salt concentration. Chlorides in aqueous solutions cause a decrease in intensity of the stretching band at about 3,250cm^{-1} but do not change the band position, while the intensity of the band at about 3,440cm^{-1} increases and its positions shifts to higher wavenumbers (e.g. Chumaevskii et al. 1999). The change in spectral shape caused by dissolved electrolytes in water was also studied by Mernagh and Wilde (1989), who introduced a "*skewing parameter*" to determine the salt concentration in the solutions. Polarisation effects on the spectra of aqueous solutions in fluid inclusions, caused by the host mineral, were not included in this study. Furić et al. (2000) introduced the Raman "*difference*" spectroscopic method to analyse chlorinity in aqueous fluids. This method was revised by Dubessy et al. (2002), using area-normalised Raman spectra. Nevertheless, the variety of contour of the Raman "stretching" water bands for equal fluids in inclusions (see Figs. 1 and 2) in quartz reduces the usefulness of Raman spectroscopy to fluid inclusion research. The present study provides a new method to rehabilitate the application of Raman spectroscopy to the analyses of aqueous solutions in fluid inclusions.

Experimental procedures and methods

Methods

Microthermometry measurements were carried out with a Linkam MDS 600 heating-freezing stage. Calibration was carried out using synthetic fluid inclusions with melting points of CO_2 at −56.6°C, the melting of H_2O ice at 0.0°C, and the critical homogenisation temperature of water at 374.0°C. Raman spectroscopy was performed with a LABRAM (ISA Jobin Yvon) instrument using a frequency-doubled 100mW Nd-YAG laser with an excitation wavelength of λ = 532.6nm. The polarisation state of the laser is consistent with the north–south direction (y-axis) of the microscope stage. All measurements were taken with a LMPlanFI 100×/0.80n.a. (Olympus) objective lens. Measurements have a precision of 1.62cm^{-1} at low $\Delta\nu$ (around 0cm^{-1}) and 1.1cm^{-1}at high $\Delta\nu$ (around 3,000cm^{-1}). For internal calibration, silicon (520cm^{-1}), polyethylene (1,062cm^{-1}, 1,128cm^{-1}, 1,169cm^{-1}, 1,295cm^{-1}, 1,487cm^{-1}, 1,439cm^{-1}, 2,848cm^{-1}, 2,881cm^{-1}), calcite (156cm^{-1}, 283cm^{-1}, 713cm^{-1}, 1,087cm^{-1}, 1,437cm^{-1}) and diamond (1,332cm^{-1}) were used. As the Raman measurement of liquid phases is very temperature sensitive, the spectra were taken at constant temperature (22°C) with varying integration times depending on the signal intensity of the inclusion. The background correction was done, by subtracting the quartz host spectrum directly adjacent to the inclusions from the signal of the fluid (see also Bakker 2004). In some cases, a second baseline correction was done with a straight-line correction. The latter was only performed in cases when the spectrum subtraction of the host mineral did not result in a straight horizontal background signal at zero intensity due to irregular fluorescence. A deconvolution with three Gaussian–Lorentzian functions was applied to each spectrum using the program Peak Fit 2002 v. 4.11 (© SYSTAT Software Inc.).

Synthesis of fluid inclusions

Fluid inclusions were synthesised in thermal shock fractures in natural Brazilian quartz according to the method of Shelton and Orville (1980) and Bodnar and Sterner (1987). The synthesis was performed in cold seal pressure vessels using a healing time of approximately 2weeks (Tables 1 and 2). The crack healing process takes place at about 600°C at varying pressures between 80MPa and 230MPa. The desired pressure of experimentation was calculated according to Zhang and Frantz (1987) using the program *ISOC* (Bakker 2003) to obtain homogenisation temperatures of about 400°C for all of the experiments. The cooling down of the pressure vessels was performed along the specific isochoric path of the experiments to prevent

Table 1 Experimental conditions of H_2O synthetic fluid inclusions in crystallographically orientated quartz cores. *P* (pressure) and *T* (temperature) represent the experimental conditions

Experiment	Orientation[a]	Duration [days]	P [MPa]	T [°C]
MYR-003	unknown	15	87.4 (±0.6)	589.1 (±1.3)
MYR-027	$[0001]$	15	86.4 (±0.6)	588.1 (±0.6)
MYR-028	$[10\bar{1}0]$	15	86.5 (±1.0)	600.2 (±0.1)
MYR-029	$[10\bar{1}0]$	15	86.1 (±0.5)	601.3 (±0.1)
MYR-041	$[2\bar{1}\bar{1}0]$	15	86.5 (±0.8)	602.2 (±0.2)
MYR-042	$[10\bar{1}1]$	15	86.4 (±0.4)	600.3 (±1.1)

[a] Line orientation parallel to the length of the cylindrical quartz core

decrepitation or stretching of the fluid inclusions. The experiments with pure water solutions (Table 1) were done with drilled quartz cores of known orientation. In experiments in the H_2O-NaCl system, the intended salinity of the added fluid was varied between 4 and 24 mass% NaCl (Table 2). After synthesis, the quartz core was cut in 1mm thick sections, doubly polished and analysed with microthermometry and Raman spectroscopy. The software *ISOC* (Bakker 2003) was used for the calculation of isochores and specific bulk densities at experimental conditions. To verify the salinity and density, microthermometry was carried out on the different solutions of the measured inclusions (Table 3). Salinity calculations from ice melting temperatures were done with the program BULK (Bakker 2003) using the equation of state of Bodnar (1993). Intended salinities (Table 2) and calculated salinities (Table 3) are slightly different due to experimental difficulties (e.g. H_2O loss during welding of the capsules). Homogenisation temperatures from low salinity experiments correspond to values calculated with the equation of state according to Zhang and Frantz (1987) using the program *LONER 38* (Bakker 2003), whereas higher salinity experiments are reproduced by the equation of state of Bodnar and Vityk (1994, program *LONER 32*, Bakker 2003). It should be noted that predicted homogenisation temperatures differ by up to 2.5% of measured values.

Table 2 Experimental conditions of NaCl-H_2O synthetic fluid inclusions in quartz. *P* (pressure) and *T* (temperature) represent the experimental conditions

Experiment	Intended mass% NaCl	Duration [days]	P [MPa]	T [°C]
MYR-008	4	16	129.9 (±0.5)	599.2 (±0.2)
MYR-009	6	14	137.2 (±1.8)	601.3 (±0.1)
MYR-010	8	14	145.7 (±1.8)	600.3 (±0.2)
MYR-011	10	15	158.5 (±0.5)	600.6 (±0.5)
MYR-012	12	14	164.8 (±0.2)	600.4 (±0.2)
MYR-013	14	14	174.9 (±0.8)	601.4 (±0.1)
MYR-017	16	15	195.2 (±0.2)	599.4 (±0.3)
MYR-015	18	14	195.7 (±0.3)	601.3 (±0.1)
MYR-016	20	14	206.2 (±0.4)	600.3 (±0.2)
MYR-018	22	14	229.7 (±1.1)	600.3 (±0.3)
MYR-004	23	14	225.6 (±0.4)	602.6 (±0.3)
MYR-019	24	14	231.3 (±0.1)	600.3 (±0.3)

Raman spectroscopic procedures

Reference Raman spectra of pure water and saline solutions (up to 24 mass% NaCl) were taken in open plastic tubes with a volume of about 480mm^3. The depth of focus was adjusted to obtain a maximum intensity of the spectrum. The deconvolved spectra were used to compare measurements made on free drops with measurements in fluid inclusions with similar salinities.

In contrast to the Raman measurement of homogeneous surfaces and pure solutions, measurements of fluid inclusions are more complicated. Inclusions with equal fluids may reveal significantly different Raman signals, i.e. amplitude intensity, due to the total inclusion volume, inclusion shape, and the depth of focus. To compensate these effects for direct comparison of individual fluid inclusions, the whole spectrum can be normalised by scaling the maximum amplitude, at approximately 3,500cm^{-1}, to equal intensities. The normalisation was done with the *LABSPEC 2.09* (Horiba, Jobin Yvon) software. Normalisation is not necessary for the comparison of peak positions and peak intensity ratios of different saline aqueous solutions.

Correlations between the geometric properties of inclusions and contour modifications in the Raman bands were investigated with five fluid inclusions in experiment MYR-019. The shape and size (including length and projected area) of these inclusions were defined according to the method of Bakker and Diamond (2006) by rotating the sample stepwise on a spindle stage.

As previously described the contour of the Raman spectra of H_2O-rich inclusions depends on the crystallographic orientation of the host quartz and the orientation of the interface (i.e. fluid inclusion wall). To investigate the crystal orientation effects on the Raman spectra, the samples were rotated over 180° in steps of 10° on the microscope stage. The rotation angles 0°, 90°, and 180° are defined as three extinction positions, where at 0° the *c*-axis is parallel to the north–south direction of the microscope stage, i.e. parallel to the laser polarisation plane. In these sets of measurements on the same inclusion, the liquid phase was always measured at the same location within the inclusion. For distinct orientations of the host crystal, quartz cores were drilled parallel to the *c*-axis, i.e. direction $[0001]$, perpendicular to the c-axis, i.e. direction $[10\bar{1}0]$ and parallel to the a-axis, i.e. direction $[10\bar{1}1]$. One orientation was drilled exactly perpendicular to one of the rhombohedral-planes $[2\bar{1}\bar{1}0]$ (see also Table 1). Influences on the Raman

Table 3 Properties of NaCl-H_2O synthetic fluid inclusions in quartz

Experiment	mass% NaCl	ρ [g/cm^3]	T_m [°C]	T_h [°C]	n
MYR-008	4.5 (±0.2)	0.52 (±0.01)	−2.7 (±0.1)	396.5 (±6.1)	30
MYR-009	5.9 (±0.2)	0.55 (±0.01)	−3.6 (±0.1)	401.7 (±3.7)	30
MYR-010	7.6 (±0.0)	0.58 (±0.00)	−4.8 (±0.0)	402.7 (±0.4)	10
MYR-011	9.7 (±0.6)	0.59 (±0.13)	−6.4 (±0.4)	402.0 (±1.5)	30
MYR-012	12.1 (±0.0)	0.67 (±0.00)	−8.3 (±0.0)	406.9 (±0.7)	10
MYR-013	13.8 (±0.1)	0.71 (±0.00)	−9.8 (±0.1)	407.3 (±1.1)	10
MYR-017	15.9 (±0.1)	0.76 (±0.00)	−12.0 (±0.1)	403.0 (±1.0)	30
MYR-015	17.9 (±0.0)	0.79 (±0.00)	−14.2 (±0.0)	398.3 (±0.2)	10
MYR-016	20.0 (±0.0)	0.82 (±0.00)	−16.8 (±0.1)	397.2 (±0.6)	10
MYR-018	22.6 (±0.1)	0.85 (±0.00)	−20.3 (±0.1)	391.7 (±1.2)	30
MYR-004	23.1 (±0.1)	0.84 (±0.01)	−21.1 (±0.1)	404.6 (±12.9)	40
MYR-019	23.2 (±0.0)	0.85 (±0.00)	−21.1 (±0.1)	388.5 (±0.5)	10

The melting temperatures of ice (T_m) and the homogenisation temperatures (T_h) were measured with microthermometry. The salinity was calculated using the experimental equation of Bodnar (1993), and density (ρ) was calculated using the equation of state of Zhang and Frantz (1987) using the software *BULK* (Bakker 2003). *n* is the number of measured inclusions.

spectra caused by the depth of the inclusions in the quartz host were investigated in experiments MYR-027 and MYR-029 (Table 1). Ten fluid inclusions at different depths in each sample were rotated through an angle of 90°, while spectra were taken every 10°.

The spectral effect of the inclusion shape (reflection polarisation effects), i.e. the orientation of the fluid-mineral interface where the laser beam enters, with respect to the laser's plane of polarisation, has been studied in a natural nearly negative-crystal-shaped inclusion (Fig. 3). This inclusion contains a H_2O-NaCl-N_2-CO_2-rich fluid mixture (composition of 5 mole% CO_2 and 95 mole% N_2 with a salt concentration of 9.23 eq. mass% NaCl). Raman measurements were taken in steps of 10° rotation (up to 180°) with focus on the planes *m, s,* r_1, r_2, r_3, and r_4 of the walls of the fluid inclusion (see Fig. 3). The Raman spectra were deconvolved with three Gaussian–Lorentzian functions.

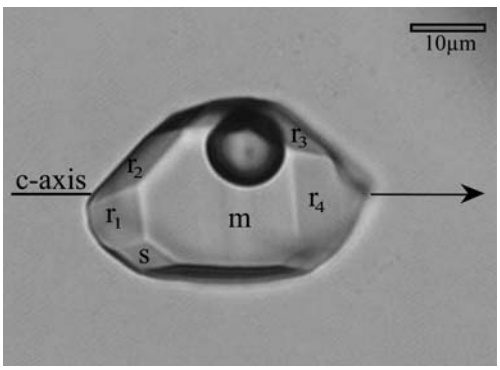

Fig. 3 Negative-crystal-shaped H_2O-N_2-CO_2-rich natural fluid inclusions with 9.23 mass% NaCl (*m*=prism-plane; *r*=rhombohedra-planes; *s*=dipyramid-plane). It has an ice melting point at −8.3°C and a clathrate melting point at 5.3°C. Raman spectral analysis reveals a composition of 5 mole% CO_2 and 95 mole% N_2. The volume fraction of the vapour phase is about 12% at room temperature

The angle between the incident laser beam and a specific fluid inclusion wall was determined by measuring the angle between the pole of the crystal faces in the wall and the pole of the plane in which the laser beam is polarised (the pole is the *x*-axis of the microscope stage), using a stereographic projection.

To better quantify the effect of birefringence on the spectral contour independently from the relative orientation of inclusion walls, a 5mm diameter hole with a depth of about 1mm was drilled in a natural quartz crystal (Fig. 4). The hole was completely filled with pure water and covered with doubly polished, orientated quartz plates (cut either parallel or perpendicular to the optical axis) of various thicknesses. This setup simulates: 1. a large fluid inclusion with a well defined orientation of the inclusion wall (i.e. the quartz cover plate); 2. the inclination of the fluid inclusion wall; and 3. the thickness of host through which the laser must pass. Raman spectra were again obtained over a total rotation of 180°.

Deconvolution

The measured spectra were deconvolved with the program PeakFit 2002 v. 4.11(© SYSTAT Software Inc.), using

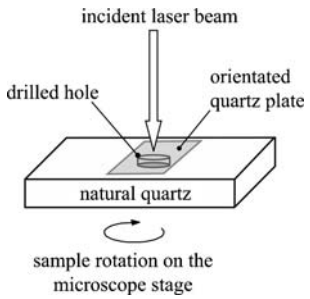

Fig. 4 The experimental setup of a fluid inclusion simulated by covering a hole (about 1 mm depth and 5 mm diameter) drilled in a quartz crystal and covered with a thin double polished quartz plate. The volume of the hole filled with solution is about 20 mm^3

Gaussian–Lorentzian functions. The best coefficient of determination, i.e. R^2 approaching 1, is obtained by these functions. The Gaussian contribution is defined by Eq 1a and 1b.

$$I_{\text{Gauss}} = a_o \cdot \exp\left[-4\ln(2) \cdot q^2\right] \tag{1a}$$

$$q = \frac{x - a_1}{a_2} \tag{1b}$$

where I_{Gauss} is the intensity, x is the relative wavenumber (cm^{-1}), a_0 is the amplitude, a_1 is the centre (cm^{-1}), i.e. the peak position, and a_2 is full width at half maximum (cm^{-1}). The Lorentzian contribution ($I_{Lorentz}$) is shown in Eq 2.

$$I_{Lorentz} = a_o \cdot \frac{1}{[1 + 4 \cdot q^2]} \tag{2}$$

Raman spectra are best described by a combination of Gaussian and Lorentzian contributions Eq 3a and 3b. This equation simply represents the intensity fractionation *(φ)*, such that $\varphi = 1$ represents a purely Gaussian contribution and $\varphi = 0$ a purely Lorentzian contribution.

$$I = \varphi \cdot I_{Gauss} + (1 - \varphi) \cdot I_{Lorentz} \tag{3a}$$

$$I = a_0 \left[\frac{\varphi \cdot \frac{\sqrt{\ln 2}}{a_2\sqrt{\ln \pi}} \cdot I_{Gauss} + (1 - \varphi) \cdot \frac{1}{\pi a_2} \cdot I_{Lorentz}}{\varphi \cdot \frac{\sqrt{\ln 2}}{a_2\sqrt{\pi}} + (1 - \varphi) \cdot \frac{1}{\pi a_2}} \right] \tag{3b}$$

Equation 3b has been selected to describe individual deconvolved band contributions of the Raman spectra (see Peak Fit v. 4.11) in our study. To avoid numerous fitting possibilities, as described in the previous paragraphs, a deconvolution with three Gaussian–Lorentzian curves as illustrated in Fig. 5 was preferred (see also Bakker 2004). It can be applied to pure H_2O as well as to brines.

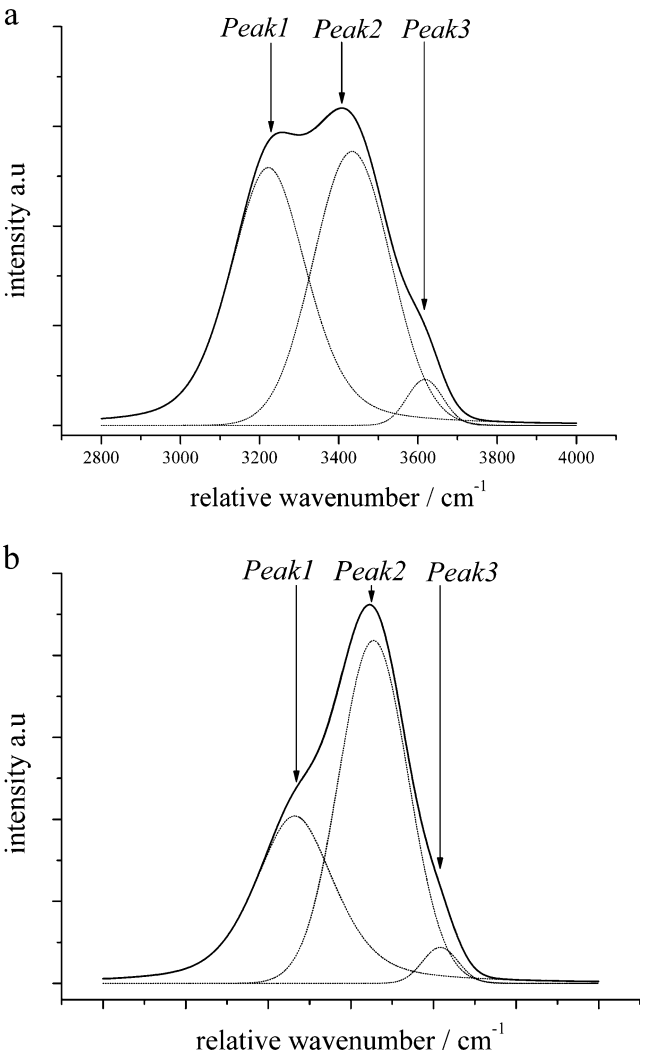

Fig. 5 Deconvolution of a Raman spectrum of pure water from sample MYR-003 **a** and of a 23 mass% NaCl-H_2O solution from sample MYR-004 **b** at room temperature by defining three Gaussian–Lorentzian components. Deconvolved peak positions for pure water are 3,222 cm^{-1} (*Peak1*), 3,433 cm^{-1} (*Peak2*) and 3,617 cm^{-1} (*Peak3*), whereas the positions for the NaCl-H_2O solution are identified at 3,266 cm^{-1} (*Peak1*), 3,454 cm^{-1} (*Peak2*) and 3,609 cm^{-1} (*Peak3*)

Results

Salinity

The most significant Raman spectral indicator for the estimation of the salinity of a free fluid (reference solutions) is the first deconvolved Gaussian–Lorentzian peak (*Peak1*, see Fig. 5). A full set of the experimental results, i.e. a_o, a_1, a_2 and φ values of all peaks, is given in the Appendix. It is possible to determine the specific relative wavenumber of *Peak1* (peak position) for fluids of different salinities (Fig. 6, solid symbols). The data show a linear increase in relative wavenumber value with increasing salinity. A linear best fit through this data results in Eq 4.

$$\Delta\nu_1 = a + b \cdot sal \tag{4}$$

where *sal* is the salinity in mass% NaCl, $\Delta\nu_1$ is the band position in relative wavenumbers, a is 3,222.8±0.3cm^{-1}, and b is 1.69±0.02cm^{-1}. Measurements of brines with similar salinities in fluid inclusions may reveal different Raman contours depending on the orientation of the host crystal and other factors. For essentially identical salinities, the deconvolved peak positions (*Peak1*) can be substantially different between the reference solutions measured in the open tubes and the fluid in inclusions (Fig. 6, shaded bars). In general, *Peak1* values in fluid inclusions are shifted to higher relative wavenumbers compared to reference solutions. The shift is illustrated with the dashed lines in Fig. 6, corresponding to maximally +27cm^{-1} for higher wavenumbers and a much smaller shift (about −6cm^{-1}) for

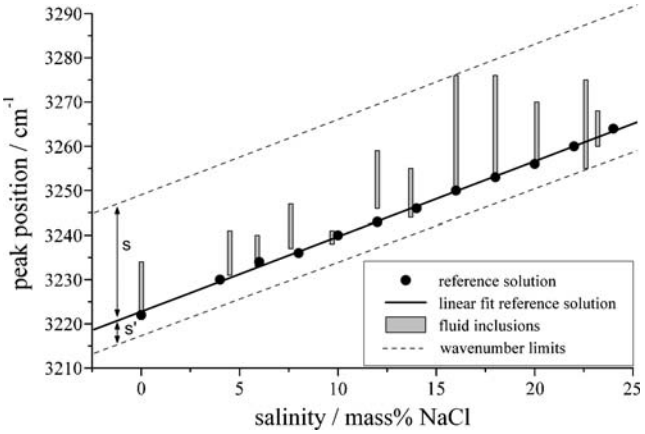

Fig. 6 Peak position of the first Gaussian–Lorentzian component (*Peak1*) as a function of salinity (mass% NaCl). Filled dots represent the peak positions measured in pure water and in saline reference solutions in open tubes. Shaded bars represent the range of peak positions measured in individual fluid inclusions in quartz over a sample rotation of 90°. *S* and *S′* represent the possible maximum offset in the band position estimation that is caused by rotation

lower wavenumbers. This spectral effect may cause an incorrect estimation of salinity in fluid inclusions by reference to Eq 4. For example, *Peak1* measured at 3,263cm^{-1} in a fluid inclusion corresponds to 16 mass% NaCl, whereas the same band position correspond to 24 mass% NaCl in the reference solution (see Fig. 6). The variation of *Peak1* per specific salinity of fluid inclusions is caused by the rotation of the sample, i.e. a variation in crystal orientation (indicatrix) with respect to the plane of polarisation of the laser beam.

Fluid inclusions

The influence of birefringence on the H_2O Raman contour was studied with respect to the crystal orientation of quartz, i.e. variation of the angle between polarisation plane of the laser beam and the axis of the ellipsoid representing refraction indices. Pure H_2O fluid inclusions were synthesised in quartz cores orientated parallel to the *c*-axis (MYR-029) as well as perpendicular to the *c*-axis (MYR-027). Due to rotation, sample MYR-029 (// *c*-axis) reveals a strong modification in the Raman bands, both in *Peak1* values and amplitude ratios belonging to *Peak2/Peak1* (open symbols in Fig. 7). Rotation results in an increase in relative wavenumbers compared to free water drops (Fig. 7a, see also Fig. 6) with a maximum and minimum about every 45°. Rotation of the crystallographic axis of quartz (either the *a*-axis or *c*-axis) to about the 30° and 120° position orientates them parallel to the laser polarisation plane, i.e. *y*-direction on the microscope stage. The wavenumber value of *Peak1* varies between 3,223cm^{-1} and 3,239cm^{-1} whereas the amplitude ratio varies between

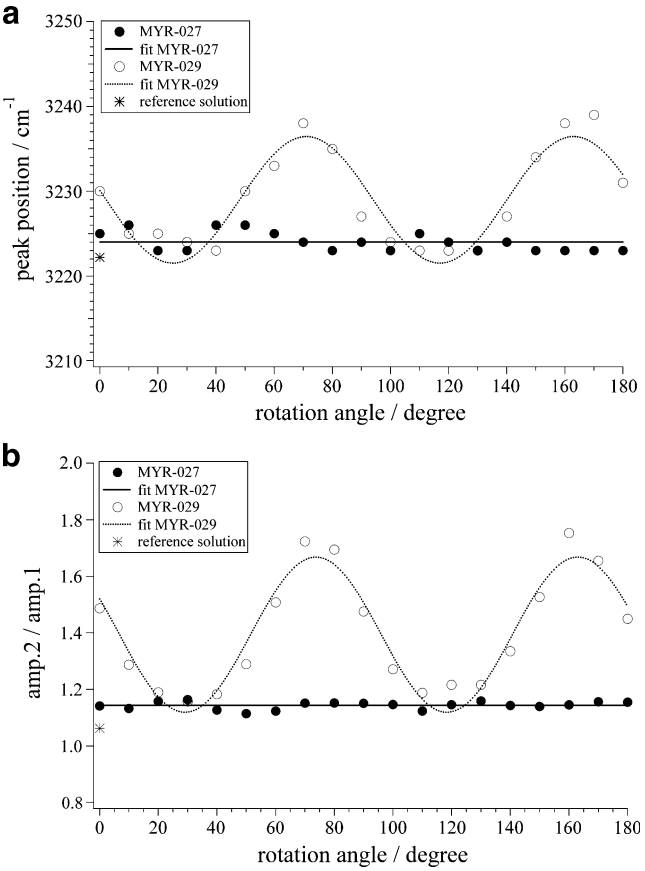

Fig. 7 Deconvolved values of *Peak1* **a** and amplitude ratios of *Peak2/Peak1* **b**, measured in synthetic fluid inclusions as a function of rotation in experiments where the sample surface is orientated perpendicular (MYR-027) and parallel to the *c*-axis (MYR-029). The continuous solid line represents a linear best fit through the data points of sample MYR-027, whereas the data points of sample MYR-029 are best represented by a sinusoidal fit (dotted line). For reference, the peak position and amplitude ratio of pure water (reference solution) are shown

1.18 and 1.72. These values are significantly different from those in the reference solution (3,222cm^{-1}, ratio of 1.06). In contrast, rotation of sample MYR-027 does not result in significant modification of the Raman bands (solid symbols in Fig. 7). Both wavenumber of *Peak1* and the amplitude ratios are approximately the same as those of the reference solution. These variations were also observed in experiments MYR-028, MYR-041 and MYR-042. However, this rotational effect does not always occur to a similar extend in a number of inclusions in these samples. It, therefore, appears that additional non-rotational effects influence the Raman spectra, which will be analysed in detail in the next paragraph.

The inclusions depth hardly affects *Peak1* (Fig. 8), using pure water in synthetic inclusions in quartz. However, the crystallographic orientation of the quartz matters. *Peak1* varies between 3,218cm^{-1} and 3,225cm^{-1} in inclusions from MYR-027 ($\perp$ *c*-axis), whereas inclusions from MYR-029

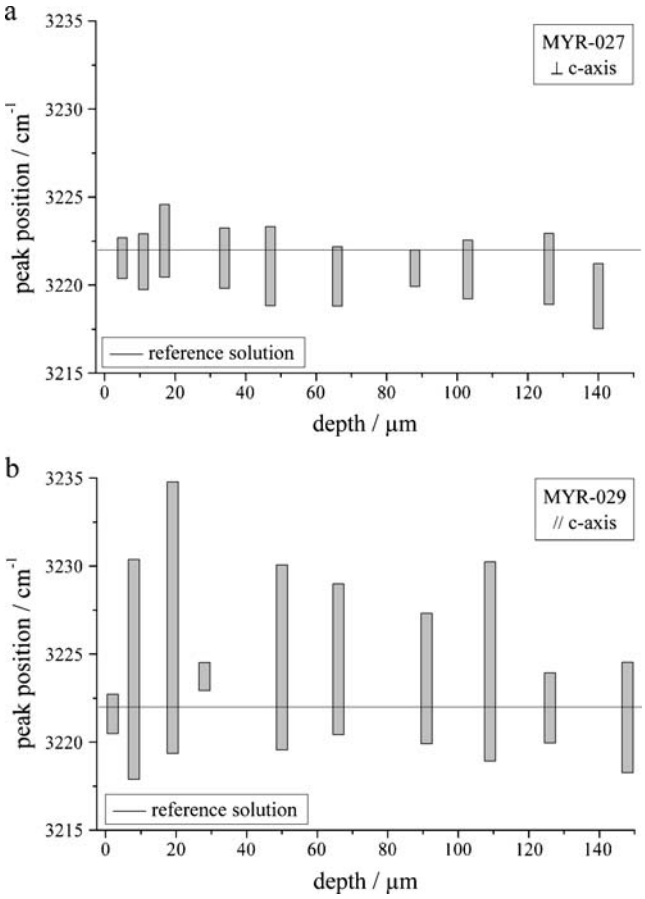

Fig. 8 Deconvolved values of *Peak1* of synthetic pure water fluid inclusions as a function of inclusion depth in the quartz host. The spectra were taken on inclusions for which the sample surface is orientated perpendicular (MYR-027, **a** and parallel to the *c*-axis (MYR-029, **b** with measurements made over a rotation of 90°. The continuous line represents the peak position of pure water (reference solution)

(// *c*-axis) reveal a much larger variation, between 3,218cm^{-1} and 3,235cm^{-1}, similar to the results illustrated in Fig. 7. This rotational variability in peak positions is mainly caused by the effect of birefringence. Within sample MYR-029 most inclusions display a large variation in peak position. However, two inclusions show a very small variation (fluid inclusions at 2µm and 28µm depth, Fig. 8b). This insensitivity to rotation must have resulted from additional effects such as interface orientation. There is no defined trend between inclusion depth and the position of the Raman bands.

The influence of size and depth of the inclusion in quartz were also studied with saline inclusions (23.2 mass% NaCl) in an inclined healed crack in experiment MYR-019 (Table 4). The variation in the evaluated peak positions results from taking spectra at different locations in several inclusions, but at the same crystallographic orientation of the quartz (without any rotation of the sample). The scatter in the data does not reveal a clear relationship between the size (area and length of the inclusion) and the *Peak1* of the fluid. The variation in *Peak1* as measured in the same inclusion indicates that another factor must affect the Raman spectra, which is not related to birefringence.

To investigate the impact of the orientation of quartz-fluid interfaces (polarisation due to reflection), a natural negative-crystal-shaped inclusion was studied (Fig. 3, Table 5). Raman measurements taken on different locations in the inclusion at the same crystallographic orientation show modifications in the spectra (Fig. 9). The orientation of this specific negative-crystal-shaped fluid inclusion implies that it is orientated parallel to the *c*-axis of the host quartz. Again, the magnitude of spectral modification depends on the rotation angle, as described in the previous paragraph, with minima and maxima in relative wavenumbers and amplitude ratios every 45°. The axes of the indicatrix coincide with the laser beam polarisation plane at these extrema. The six locations show a variety of spectra (Fig. 9, Table 5). The horizontal interface (*m*) is more sensitive to the rotation angle (large modification in the Raman contour), whereas steeper interfaces (e.g. r_4) are less influenced (Fig. 9, Table 5). There is no clear relationship between the variability of the spectra and the angle between the interface plane and the polarisation plane of the laser beam. This interface-orientation effect was also seen in the

Table 4 Properties represented by the maximum areas and lengths of fluid inclusions in experiment MYR-019

Inclusion	Peak position (*Peak1*) (cm^{-1})	Area (µm^2)	Length (µm)	T_m(ice) (°C)	T_m(HH) (°C)	T_h (°C)
FI2	3,264 to 3,266	177.0	23.8	−21.1	−18.9	390.8
FI4	3,261 to 3,269	284.2	29.7	−21.1	−19.0	391.5
FI5	3,270 to 3,273	234.3	32.5	−21.0	−19.0	391.3
FI7	3,268 to 3,282	117.2	16.9	−21.1	−19.1	390.3
FI9	3,260 to 3,261	132.1	14.8	−21.0	−18.9	393.0

The melting temperatures of ice "T_m*(ice)*" and hydrohalite "T_m*(HH)*" as well as the homogenisation temperatures (T_h) were recorded with microthermometry. The variation in the evaluated peak positions results from measurements taken at different locations in the fluid inclusions at the same crystallographic orientation of the host mineral.

Table 5 Deconvolved values of *Peak1* of the natural negative-crystal-shaped fluid inclusion during the rotation of the sample up to 180°

Rotation (°)	m (cm^{-1})	s (cm^{-1})	r_1 (cm^{-1})	r_2 (cm^{-1})	r_3 (cm^{-1})	r_4 (cm^{-1})
0	3,234 (±2)	3,236 (±2)	3,236 (±2)	3,232 (±2)	3,235 (±2)	3,234 (±2)
15	3,234 (±2)	3,232 (±2)	3,236 (±2)	2,340 (±3)	3,236 (±2)	3,234 (±2)
30	3,241 (±2)	3,240 (±2)	3,241 (±2)	3,246 (±3)	3,242 (±3)	3,235 (±2)
45	3,244 (±2)	3,239 (±2)	3,243 (±2)	3,254 (±4)	3,246 (±3)	3,237 (±2)
60	3,237 (±2)	3,236 (±2)	3,239 (±2)	3,238 (±3)	3,240 (±3)	3,234 (±2)
75	3,232 (±2)	3,233 (±2)	3,234 (±2)	3,233 (±2)	3,233 (±3)	3,231 (±2)
90	3,233 (±2)	3,230 (±2)	3,231 (±2)	3,233 (±2)	3,238 (±3)	3,234 (±2)
120	3,242 (±2)	3,235 (±2)	3,239 (±2)	3,244 (±3)	3,233 (±3)	3,236 (±2)
150	3,234 (±2)	3,236 (±2)	3,237 (±2)	3,240 (±3)	3,235 (±3)	3,235 (±2)
180	3,231 (±2)	3,231 (±2)	3,233 (±2)	3,234 (±2)	3,237 (±3)	3,232 (±2)

Measurements were made at six different locations (*m, s,* r_1, r_2, r_3, and r_4), as shown in Fig. 3.

synthetic inclusions in sample MYR-019 (Table 4), which have irregular morphologies. Note that this orientation phenomenon was not observed in inclusions where the sample surface is orientated perpendicular to the optical axis.

Simulations

By analysing simulated inclusions (Fig. 4), the influence of birefringence was determined independently from the interface effects. The spectrum of pure liquid water was strongly influenced in the experiment where the quartz plate, covering the water drop in the quartz cavity, had an orientation parallel to the *c*-axis [0001] and one a-axis $[10\bar{1}0]$. Figure 10 illustrates the systematical modifications of the Raman contour during the rotation of the sample from 0° to 45°. The typical Raman spectrum of pure water (as illustrated in Fig. 5a) was only observed when the *c*-axis (shown with 0° in Fig. 10) or *a*-axis was orientated exactly parallel to the laser beam's polarisation plane, whereas in all other orientations spectral variations were recorded. The greatest modification in the deconvolved peak position and amplitude ratio was recorded at a rotation angle of 45° (see Fig. 10). Experiments where the quartz plate was orientated perpendicular to the *c*-axis did not show significant rotation-dependent modifications in the spectra. This observation confirms that birefringence is a major actuator of this variability in spectra contour, similar to the results with synthetic fluid inclusions (Fig. 7).

The rotation-induced variation in Raman bands for pure H_2O with increasing depth in the simulated inclusion is illustrated in Fig. 11. This set of analyses was done using quartz plates of different thickness and orientation (see Fig. 4). The wavenumber value of *Peak1* decreases systematically with increasing depth in experiments with quartz plates perpendicular (MYR-027) and parallel (MYR-029) to the *c*-axis. As expected from the behaviour of the Raman spectra of synthetic fluid inclusions (see Fig. 8), the rotation-induced variation is small for quartz plates perpendicular to the *c*-axis (Fig. 11a). In experiments with quartz plates orientated parallel to the *c*-axis (Fig. 11b), the variation is much greater for shallow inclusions (3,218cm^{-1} to 3,233cm^{-1}), and decreases drastically towards deeper

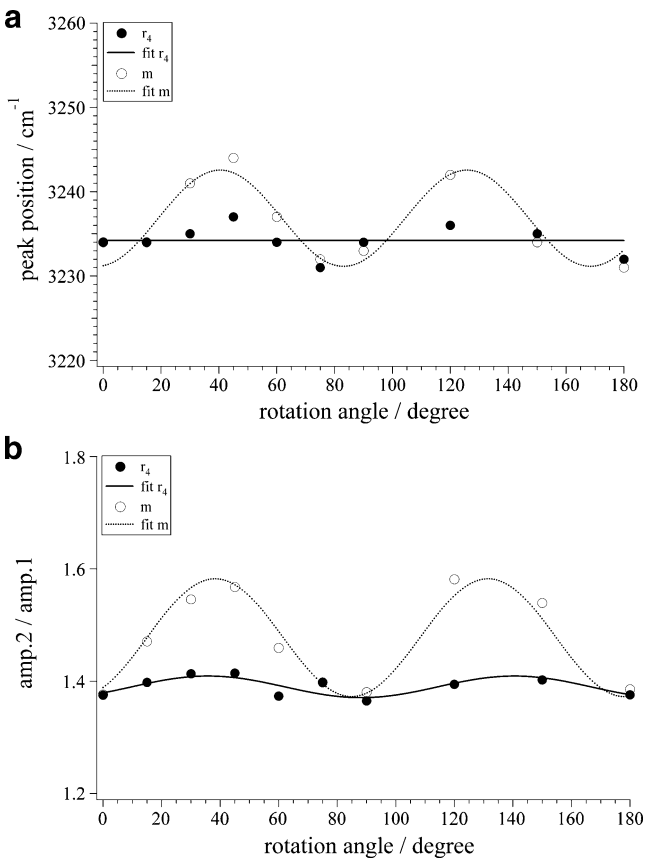

Fig. 9 Deconvolved values of *Peak1* **a** and amplitude ratios of *Peak2/Peak1* **b** as a function of rotation angle measured in the same negative-crystal-shaped inclusion (see Fig. 3) on two different planar interfaces (r_4=rhombohedra-plane; *m*=prism-plane). The continuous solid line represents the linear best fit through the data points of plane r_4 whereas the data points of plane *m* are best represented by a sinusoidal fit (dotted line)

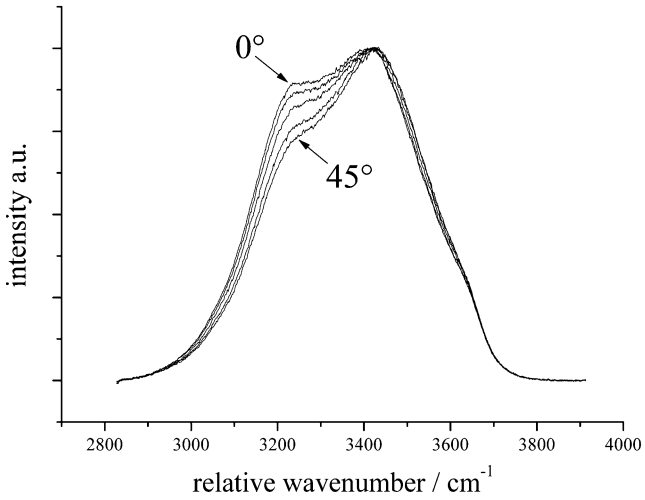

Fig. 10 Influence of the polarisation effect on the Raman stretching band of water due to the birefringence of quartz evidenced by the rotation of the quartz covering plate of simulated inclusions. At 0° the quartz plate was orientated parallel to the *c*-axis (north-south direction of the microscope stage which is parallel to the laser polarization plane) and was then stepwise rotated to 45°. See text for further details

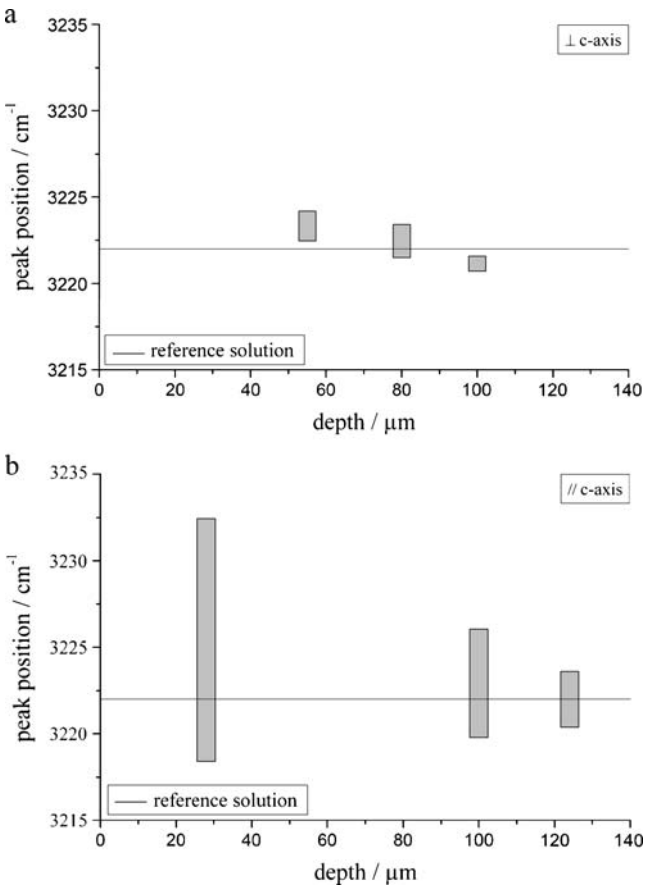

Fig. 11 Deconvolved values of *Peak1* of the simulated pure water fluid inclusions, as measured with different thickness of the quartz cover plates, orientated perpendicular to the *c*-axis **a** and parallel to the *c*-axis **b** with measurements made over a rotation of 90° (shaded bars). The continuous line represents the peak position of pure water (reference solution)

levels. Therefore, the effect of birefringence is minimised with increasing depth. The behaviour shown in Fig. 11 is different from the results obtained on multiple natural fluid inclusions (Fig. 8), but not in contrast because the additional effects such as reflection polarisation are constant for all measurements.

Discussion

Normalisation and ratios

Spectra obtained on different objects of similar material can be compared on the basis of band position and intensity. The intensity of the Raman signal depends on a variety of factors, such as the instrumental setup, surface irregularities, material densities, crystal orientation, volume of matter, and the inherent Raman scattering cross-section. However, for identical materials, the relative wavenumber position of peaks remains approximately constant. Because fluid inclusions are detected below the surface of the host, a change in depth results in a change in intensity of the Raman signal. In order to compare visually the Raman spectra among a series of fluid inclusions, the spectra have, therefore, to be normalised. Subsequently, the normalised spectra can be used to analyse salinity effects and properties of the host crystal that may influence the morphology of the spectra. For the analysis of peak positions and amplitude ratios, this normalisation is not required. In contrast, fluids that are directly measured in standard solutions with the same apparatus do not need to be normalised. Those spectra reveal directly both intensity and wavenumber shifts as a result of a variable salinity (see Fig. 6).

Three purely geometrical methods have been proposed in literature to analyse the Raman spectra of aqueous solutions at room temperatures: 1. Skewing parameter (Mernagh and Wilde 1989); 2. Raman difference spectroscopy (Furić et al. 2000; Dubessy et al. 2002); 3. Deconvolution (Bakker 2004).

The method of Mernagh and Wilde (1989) does not require normalisation of the obtained spectra, because it is based on ratios of the geometrically defined properties of individual spectra (Fig. 12a). The skewing parameter is relatively easy to obtain from raw spectra, i.e. directly obtained from the instrument. The accuracy of the salinity calculation based on this method is about 3 mass% and it was only tested for the binary H_2O-NaCl fluid system.

Normalisation of spectra is required in the method of Dubessy et al. (2002) because the spectrum of the sample has to be compared to a reference spectrum (see Furić et al., 2000). This normalisation is obtained by dividing the

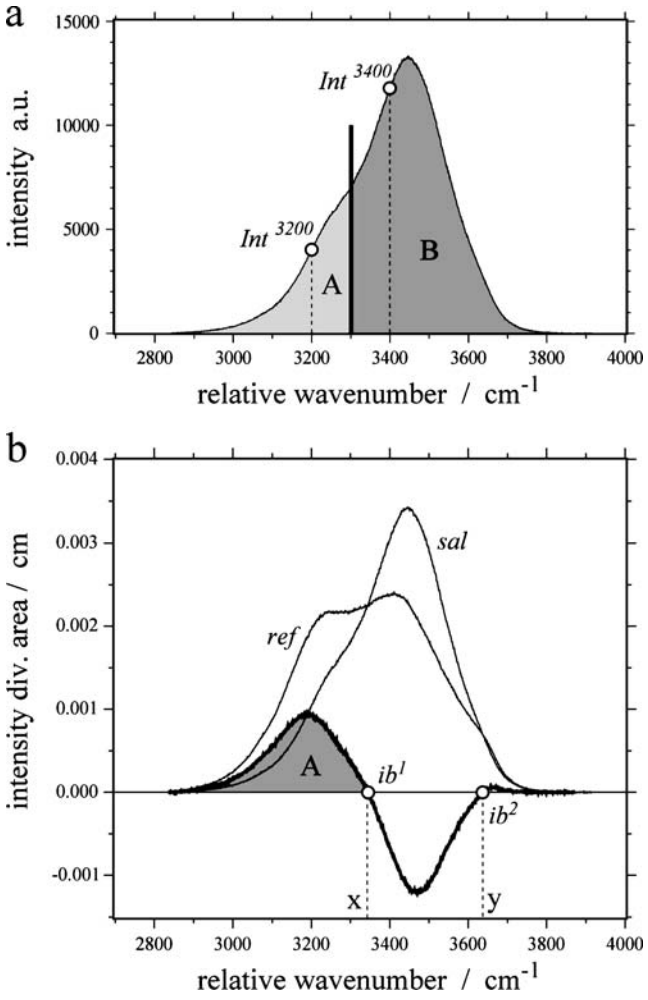

Fig. 12 **a** The method described by Mernagh and Wilde (1989), i.e. by dividing the O-H Raman profile into two halves at 3,300 cm^{-1} (thick solid vertical line). The ratio of the area *A* (between 2,800 cm^{-1} and 3,300 cm^{-1}) over area *B* (between 3,300 cm^{-1} and 3,800 cm^{-1}) is used to express symmetric and anti-symmetric components of the spectra. The ratio of the intensity at 3,200 cm^{-1} (int^{3200}) over intensity at 3,400 cm^{-1} (int^{3400}) is used to calculate the cation effect. See Mernagh and Wilde (1989) for further details. **b** The method described by Dubessy et al. (2002) using Raman difference spectroscopy. The *y*-axis represents an "intensity div area" variable, which expresses the normalised values of the spectra (in cm). The normalised spectra of a fluid inclusion (sal) are subtracted from that of the H_2O reference solution (ref). The area *A* of the resulting curve is a measure for the salinity. The "isobestic points" (ib^1 and ib^2) may reveal the type of dissolved salt, corresponding to the wavenumber equivalent *x* and *y* . See Dubessy et al. (2002) for further details

intensity at each wavenumber position by the total area of the spectrum in order to obtain one unit area (Fig. 12b). Additionally, this method includes the possibility to estimate the type of dissolved salts from "isobestic points". However, the wavenumber "equivalent" for specific one-component salts may coincide or be within a few cm^{-1} (within the accuracy) of each other, and the "isobestic points" of aqueous solutions with multiple salt components are unknown.

In this study, the normalisation of maximum intensity was only applied to visualise the changes in morphology of the Raman spectra due to host mineral properties. The deconvolved Raman spectra, according to the method of Bakker (2004), are not normalised for the analysis of peak positions and amplitude ratios. Reference fluids can be directly compared to the analysis of natural fluid inclusions. Similar to the method of Mernagh and Wilde (1989), the method can be applied to raw spectra and is also limited to the binary H_2O-NaCl system.

Birefringence polarisation

The most obvious explanation of variation in the Raman spectra of fluid in inclusions is the effect on the polarisation of the incident laser beam caused by the orientation of the host crystal (see also Dubessy et al. 2002). The Raman spectrum of fluid phases in inclusions is defined not only by the fluid phase itself: the laser light has to cross the host mineral, which causes additional polarisation effects in birefringent minerals.

Mernagh and Wilde (1989) did not consider the optical properties of birefringent materials in their study of salinity effects on the Raman spectrum of aqueous fluids. Consequently, their linear regression with the "skewing parameter" has limited application to the determination of the salinity of natural inclusions in quartz. Dubessy et al. (2002) suggested to minimise these effects by using a depolarised laser or to orientate an axis of the indicatrix of birefringent host minerals parallel to the spectrometer slit. Our results (Fig. 7) have confirmed that Raman spectra that are influenced only by the birefringence of the host mineral are preferably analysed such that the host crystal has its optical axis orientated parallel to the polarisation plane of the laser. Our results also reveal that the lowest value of *Peak1* obtained from the rotation-controlled variation in the spectrum of a fluid inclusion (Fig. 7) best matches the *Peak1* in the reference solution. Peak positions of sample MYR-027 (sample surface is orientated perpendicular to the optical axis) are comparable to those of the reference solution of pure water. The minimum in the periodic function for sample MYR-029 (sample surface is orientated parallel to the optical axis) approaches the *Peak1* of the reference fluid (see Fig. 7a)

Reflection polarisation

Previous studies have paid little attention to polarisation effects of the laser beam due to the orientation of the quartz-fluid interface. The results given in Fig. 9 demonstrate that this factor cannot be ignored in the interpretation of salinities from Raman spectra of aqueous solutions in natural fluid inclusions. Reflection of the incoming light

(laser beam) at the quartz-fluid interface induces polarisation effects as well (e.g. Tipler 1991). Figure 9 also illustrates that the orientation of the quartz host is a factor in the over-all effect. The rotation angle 0°, 90°, and 180° correspond to three extinction positions of quartz. Therefore, the reflection polarisation is partly coupled to the birefringence polarisation. According to Eq 4, the wavenumber of *Peak1* measured in a fluid with about 9 mass% NaCl is 3,238±1cm^{-1}. Figure 9 a illustrates for a natural inclusion of this composition a range in wavenumber values of 3,232cm^{-1} to 3,244cm^{-1} that can be derived from the m-interface, and a smaller range for the r_4-interface (3,231cm^{-1} to 3,237cm^{-1}). Figure 6 indicates that in such an inclusion with 9 mass% NaCl wavenumbers can vary between 3,232cm^{-1} to 3,265cm^{-1}, depending on the orientation of the host crystal. Therefore, the true salinity of this inclusion could not be directly estimated from the Raman spectrum of the aqueous solution simply by reference to values obtained on standard solutions. Gases dissolved in the aqueous solution have an additional effect on the variety of the Raman stretching band morphology.

Inclusion depth

Quantification of the variation in Raman band morphology due solely to the depth of an inclusion in the quartz host is complicated (Fig. 8) by additional polarisation phenomena that may camouflage this effect. However, the results from simulated inclusions (Fig. 11) illustrate a correlation between the depth of the inclusion and modifications in the Raman bands. Higher *Peak1* values are obtained from shallow inclusions when compared to deeper inclusions of the same composition, regardless of whether the quartz cover was cut parallel or perpendicular to the *c*-axis. In the experiment in which the cover plate was cut parallel to the *c*-axis the rotation-induced variation caused by birefringence (Fig. 11b) decreases with increasing depth. Consequently, the deeper simulated inclusions reveal *Peak1* values that approach the value of the reference solution, independent of crystal orientation.

Applications for fluid inclusion studies

This study has shown that a large variety of salinities may give Raman spectra with similar band morphologies in the 2,800cm^{-1} to 3,800cm^{-1} region. Therefore, the application of Raman spectral analysis to aqueous solutions containing a salt in natural fluid inclusions is still limited. As already indicated by Dubessy et al. (2002), an independent method is necessary to obtain the cation ratios before the salinity of natural inclusions can be determined via Raman spectroscopy. For example, the Raman spectra of salt hydrates in frozen inclusions reveal the major cations dissolved in the aqueous solution (e.g. Dubessy et al. 1982; Bakker 2004).

Microthermometry remains the main tool for analysing the salinity of natural fluid inclusions. Raman spectroscopy may be used to verify microthermometric results or to specify in more detail the analysed phase changes (e.g. Bakker 2004; Gasparrini et al. 2006). Furthermore, inclusions that are too small for optical microthermometric analysis (smaller than 2μm diameter) can be investigated with Raman spectroscopy. For these inclusions, Raman spectroscopy offers a tool to specify the phases that are present within the inclusions. The aqueous phase can be analysed with Raman spectroscopy to obtain its salinity according to our method.

Natural fluid inclusions may be hosted in birefringent minerals such as quartz. The orientation of the sample and the shape of the inclusion itself will influence the morphology of the Raman band contour. For this reason, the orientation of the host should be controlled during measurements. In optically uniaxial minerals like quartz the best way to operate is to orientate the sample surface perpendicular to the *c*-axis, where birefringence and reflection polarisation do not influence the spectra. Another possibility would be to orientate the sample surface in an extinction position, such that the *c*-axis or *a*-axis is orientated parallel to the laser polarisation plane, to obtain the typical spectrum. The orientation of quartz grains can only be evaluated with Raman spectrometers equipped with an integrated optical microscope that has the option to use crossed polarisers. The orientation of the crystal in natural samples is often very difficult to determine due to the absence of this experimental setup. When the orientation of the host mineral cannot be determined or optimised, the inclusions under analysis have to be rotated through at least 90° and spectra obtained at regular intervals. The spectra must be deconvolved into three bands using Gaussian–Lorentzian functions. The lowest position derived for the first (*Peak1*) of the three bands can be referenced to a Raman calibration curve for salinity of standard solutions. If neither optimal orientation of the sample nor multiple analysis through 90° of rotation is possible, the acquisition of a spectrum of the O-H stretching region in an aqueous solution in a birefringent host will not enable determination of its salinity. Indeed, comparison of such a randomly derived spectrum to spectra of standard solutions will result in erroneous salinity values.

Conclusions

The Raman spectrum of aqueous solutions (H_2O-NaCl mixtures) can be analysed by deconvolution into three Gaussian–Lorentzian contributions. Pure H_2O has peak

positions at 3,223cm^{-1} (*Peak1*), 3,433cm^{-1} (*Peak2*), and 3,617cm^{-1} (*Peak3*). The presence of salt in the aqueous solutions has significant influence on the morphology of the spectra. The (shifted) position of the first peak (*Peak1*) can be used to determine the salinity of the aqueous solution by comparing it with reference spectra taken on standard solutions.

For an aqueous solution in a fluid inclusion, the morphology of a Raman spectrum produced by a polarised laser beam is influenced by the optical properties of the host crystal, by the orientation of the quartz-fluid interface, and by the depth of the inclusion within the sample.

The maximum variation in *Peak1* values for NaCl-bearing aqueous solutions that is defined by all polarisation effects is about 33cm^{-1}. Due to birefringence, the estimated *Peak1* values of pure H_2O fluid inclusions in quartz can vary between 3,223cm^{-1} and 3,239cm^{-1}. Polarisation caused by reflection, which depends on the orientation of the quartz-fluid interface, results in a variation of about 14cm^{-1} relative wavenumbers. Horizontal interfaces reveal a larger polarisation effect than steeper interfaces, independent of the relative orientation of the optical indicatrix of the host mineral.

The individual effects of birefringence, interface orientation, and depth of the inclusion below the mineral surface have been evaluated with simulated fluid inclusions, i.e. by drilling a small hole in quartz and covering it with a doubly polished quartz plate of selected thickness and crystallographic orientation. The variation in *Peak1* due to birefringence is smaller for quartz plates cut perpendicular to the *c*-axis (3,320cm^{-1} to 3,224cm^{-1}) than for quartz plates cut parallel to the *c*-axis (3,220cm^{-1} to 3,232cm^{-1}). The effect of birefringence is reduced with increasing depth.

For natural inclusions, the morphology of the Raman spectra of aqueous solutions is simultaneously modified by all of these effects. The possibility to orientate the optical axis of the quartz crystal parallel to the plane of polarisation of the laser beam results in spectra of aqueous inclusions that have almost the same morphology as spectra of reference solutions of the same composition. Raman equipment that does not offer this possibility can be used to analyse the salinity of aqueous solutions by acquiring multiple spectra throughout at least 90° rotation of the sample and determining the lowest peak position of the deconvolved Gaussian–Lorentzian contributions (*Peak1*).

Acknowledgements The research work is funded by the Austrian Science Fund (FWF, P18209-B06). We would like to thank the University of Graz (Institute for Earth Sciences, Department of Mineralogy and Petrology) for the possibility using their Raman equipment for measurements of the reference solutions. Yvan Coquinot is thanked for helping with the synthesis of fluid inclusions. R. Burruss, J. Dubessy, T. Mernagh, I-Ming Chou, and J. D. Pasteris are kindly acknowledged for reviewing this manuscript.

Appendix

Table 6 Properties of the deconvolved peaks obtained from the reference solutions using the program PeakFit 2002 v. 4.11 (© SYSTAT Software Inc.)

	Peak	a_0	a_1	a_2	φ
H_2O	1	12,936 (±90)	3,222 (±1)	228 (±1)	0.52 (±0.01)
	2	13,741 (±58)	3,433 (±0)	230 (±2)	1.00 (0.02)
	3	2,310 (±87)	3,617 (±1)	106 (±2)	1.00 (0.13)
2 mass% NaCl	1	12,608 (±91)	3,227 (±1)	230 (±1)	0.53 (±0.01)
	2	14,381 (±62)	3,437 (±0)	227 (±2)	1.00 (±0.02)
	3	2,307 (±91)	3,617 (±1)	105 (±2)	1.00 (±0.13)
4 mass% NaCl	1	12,518 (±92)	3,230 (±1)	230 (±1)	0.53 (±0.01)
	2	15,121 (±65)	3,440 (±0)	224 (±2)	1.00 (±0.02)
	3	2,312 (±95)	3,617 (±1)	104 (±2)	1.00 (±0.14
6 mass% NaCl	1	12,117 (±88)	3,234 (±1)	231 (±1)	0.52 (±0.01)
	2	15,491 (±64)	3,443 (±0)	222 (±2)	1.00 (±0.02)
	3	2,251 (±92)	3,617 (±1)	103 (±2)	1.00 (±0.14)
8 mass% NaCl	1	12,070 (±91)	3,236 (±1)	232 (±1)	0.52 (±0.01)
	2	16,349 (±67)	3,445 (±0)	220 (±2)	1.00 (±0.02)
	3	2,238 (±96)	3,617 (±1)	102 (±2)	1.00 (±0.14)
10 mass% NaCl	1	11,647 (±89)	3,240 (±1)	232 (±1)	0.54 (±0.01)
	2	16,640 (±69)	3,447 (±0)	217 (±2)	1.00 (±0.02)
	3	2,175 (±96)	3,616 (±1)	100 (±2)	1.00 (±0.15)
12 mass% NaCl	1	11,295 (±87)	3,243 (±1)	230 (±1)	0.51 (±0.01)
	2	17,223 (±66)	3,448 (±0)	215 (2)	1.00 (±0.02)
	3	2,149 (±93)	3,617 (±1)	99 (±2)	1.00 (±0.15)

Table 6 (continued)

	Peak	a_0	a_1	a_2	φ
14 mass% NaCl	1	11,390 (±92)	3,246 (±1)	231 (±1)	0.52 (±0.01)
	2	18,374 (±72)	3,450 (±0)	213 (±2)	1.00 (±0.02)
	3	2,185 (±99)	3,616 (±1)	99 (±2)	1.00 (±0.15)
16 mass% NaCl	1	11,402 (±95)	3,250 (±1)	231 (±1)	0.50 (±0.01)
	2	19,498 (±76)	3,451 (±0)	210 (±1)	1.00 (±0.02)
	3	2,239 (±102)	3,616 (±1)	98 (±2)	1.00 (±0.15)
18 mass% NaCl	1	10,687 (±90)	3,253 (±1)	229 (±1)	0.48 (±0.01)
	2	19,269 (±73)	3,452 (±0)	207 (±1)	1.00 (±0.02)
	3	2,139 (±98)	3,616 (±1)	96 (2)	1.00 (0.15)
20 mass% NaCl	1	10,664 (±93)	3,256 (±1)	228 (±1)	0.49 (±0.01)
	2	20,400 (±76)	3,453 (±0)	204 (±1)	1.00 (±0.02)
	3	2,215 (±100)	3,616 (±1)	97 (±2)	1.00 (±0.15)
22 mass % NaCl	1	10,605 (±104)	3,260 (±1)	228 (±1)	0.42 (±0.01)
	2	20,558 (±87)	3,453 (±0)	200 (±1)	1.00 (±0.02)
	3	2,184 (±111)	3,617 (±1)	102 (±2)	1.00 (±0.16
24 mass% NaCl	1	10,210 (±106)	3,264 (±1)	227 (±1)	0.42 (±0.01)
	2	20,915 (±90)	3,455 (±0)	197 (±1)	1.00 (±0.02)
	3	2,196 (±110)	3,617 (±1)	102 (±2)	1.00 (±0.15)

a_o is peak intensity, a_1 is peak position, a_2 is half width at full maximum, and ϕ the fraction of the Gaussian component (see text for details.

References

Bakker RJ (2003) FLUIDS 1: Computer programs for analysis of fluid inclusion data and for modelling bulk fluid properties. Chem Geol 194:3–23

Bakker RJ (2004) Raman spectra of fluid and crystal mixtures in the system H_2O, H_2O-NaCl and H_2O-$MgCl_2$ at low temperatures: applications to fluid inclusion research. Can Mineral 42:1283–1314

Bakker RJ, Diamond LW (2006) Estimation of volume fractions of liquid and vapour phases in fluid inclusions, and definition of inclusion shape. Am Mineral 91:635–657

Bodnar RJ (1993) Revised equation and table for determining the freezing point depression of H_2O-NaCl solutions. Geochim Cosmochim Acta 57:683–684

Bodnar RJ, Sterner SM (1987) Synthetic fluid inclusions. In: Ulmer GC, Barnes HL (eds) Hydrothermal experimental techniques. John Wiley & Sons, New York, pp 423–457

Bodnar RJ, Vityk MO (1994) Interpretation of microthermometric data for H_2O-NaCl- fluid inclusions. In: de Vivo B, Frezotti ML (eds) Fluid inclusion in minerals: methods and applications. Short Course, IMA, pp 117–130

Burke EAJ (2001) Raman microspectrometry of fluid inclusions. Lithos 55:139–158

Carey DM, Korenowski GM (1998) Measurement of the Raman spectrum of liquid water. J Chem Phys 108–7:2669–2675

Chumavskii NA, Rodnikova MN, Sirotkin DA (1999) Raman spectra of light and heavy water in the O-H and O-D stretching vibrations region. J Mol Liq 82:39–46

Chumavskii NA, Rodnikova MN, Sirotkin DA (2001) Cationic effect in aqueous solutions of 1:1 electrolytes by Raman spectral data. J Mol Liq 91:81–90

Dubessy J, Audeoud D, Wilkins R, Kosztolanyi C (1982) The use of the Raman microrobe MOLE in the determination of the electrolytes dissolved in the aqueous phase of fluid inclusions. Chem Geol 37:137–150

Dubessy J, Lhomme T, Boiron MC, Rull F (2002) Determination of chlorinity in aqueous fluids using Raman spectroscopy of the strecthing band of water at room temperature: Application to fluid inclusions. Appl Spectrosc 56:99–106

Dubessy J, Boiron MC, Moissette A, Monnin C, Sretenskaya N (1992) Determinations of water, hydrates and pH in fluid inclusions by micro-Raman spectroscopy. Eur J Mineral 4:885–894

Frantz JD, Dubessy J, Mysen B (1993) An optical cell for Raman spectroscopic studies of supercritical fluids and application to the study of water to 500°C and 2000 bar. Chem Geol 106:9–26

Furić K, Ciglenečki B, Ćosović B (2000) Raman spectroscopic study of sodium chloride water solutions. J Mol Struct 550–551:255–234

Gasparrini M, Bakker RJ, Bechstädt T (2006) Characterization of dolomitizing fluids in the Carboniferous of the Cantabrian zone (NW Spain): A fluid inclusion study with cryo-Raman spectroscopy. J Sed Res 76:1304–1322

Gopalakrishnan S, Jungwirth P, Tobias DJ, Allen H (2005) Air-liquid interfaces of aqueous solutions containing ammonium and sulfate: spectroscopic and molecular dynamics studies. J Phys Chem B 109:8861–8872

Li R, Jiang Z, Chen F, Yang H, Guan Y (2004) Hydrogen bonded structure of water and aqueous solutions of sodium halides: a Raman spectroscopic study. J Mol Struct 707:83–88

Mernagh TP, Wilde AR (1989) The use of the Raman microprobe for the determination of salinity in fluid inclusions. Geochim Cosmochim Acta 53:765–771

PeakFitTM 4.11 for Windows® User`s manual (2002) SYSTAT software Inc. 1/4–1/9

Ratcliffe CI, Irish DE (1982) Vibrational spectral studies of solutions at elevated temperatures and pressures. 5. Raman studies of liquid water up to 300°C. J Phys Chem 86:4897–4905

Roedder E (1984) Fluid inclusions. Rev Mineral 12:305–584

Rull F (2002) Structural investigation of water and aqueous solutions by Raman spectroscopy. Pure Appl Chem 74–10:1859–1870

Rull F, de Saja JA (1986) Effect of electrolyte concentration on the Raman spectra of water in aqueous solutions. J Raman Spectrosc 17:167–172

Shelton KL, Orville PM (1980) Formation of synthetic fluid inclusions in natural quartz. Am Mineral 65:1233–1236

Tipler PA (1991) Physics for scientists and engineers. 3rd edition Worth, New York, pp 1047–1048

Turell G, Corset J (1996) Raman microscopy. Development and applications. Academ Press Hartcourt & Company, London, pp 463

Walrafen GE (1962) Raman spectral studies of the effects of electrolytes on water. J Chem Phys 36:1035–1042

Zhang YG, Frantz JD (1987) Determination of the homogenization temperatures and densities of supercritical fluids in the system NaCl-KCl-$CaCl_2$-H_2O using synthetic fluid inclusions. Chem Geol 64:335–350